Icarus 275 (2016) 221–231

Contents lists available at ScienceDirect

Icarus

journal homepage: www.elsevier.com/locate/icarus

Detecting meteoroid streams with an in-situ dust detector above an airless body

Jamey R. Szalay[a,*], Mihály Horányi[b,c,d]

[a] Southwest Research Institute, 6220 Culebra Rd, San Antonio, TX 78238, USA
[b] Laboratory for Atmospheric and Space Physics, 1234 Innovation Dr., Boulder, CO 80303, USA
[c] Institute for Modeling Plasma, Atmospheres, and Cosmic Dust, 3400 Marine St., Boulder, CO 80303, USA
[d] Department of Physics, University of Colorado Boulder, 392 UCB, Boulder, CO 80309, USA

ARTICLE INFO

Article history:
Received 5 October 2015
Revised 22 March 2016
Accepted 16 April 2016
Available online 25 April 2016

Keywords:
Moon
Interplanetary Dust
Meteors

ABSTRACT

The Lunar Dust Experiment (LDEX), aboard NASA's Lunar Atmosphere and Dust Environment Explorer (LADEE) successfully mapped the dust density distribution over the lunar surface up to an altitude of ~ 250 km. LDEX detected dust grains launched off the surface in ejecta plumes generated by impacts of cometary and asteroidal micrometeoroids striking the Moon. While on average LDEX detected particles at a rate of 1 min^{-1}, periodically it measured bursts of particles at a rate exceeding the average value by up to two orders of magnitude. The timing and location of the most intense period of bursts is used here to independently determine the radiant for the Geminids meteoroid stream. The method is proposed to be of general interest to characterize meteoroid streams bombarding any of the airless bodies in the solar system using in-situ dust detectors.

1. Introduction

Every planetary body in the inner solar system is continually bombarded by interplanetary dust particles (IDP) originating primarily from asteroid collisions and cometary activities. Thick atmospheres protect Venus, Earth, and Mars, ablating the incoming IDPs into 'shooting stars' that rarely reach the surface. The surfaces of airless bodies near 1 AU are directly exposed to the high-speed, $v \gg 1$ km/s, impacts of IDPs with a characteristic radius of $a \simeq 100$ μm and mass flux of $F \simeq 1.5 \times 10^{-15}$ kg/m^2/s (Grün et al., 1985). The total mass influx to Earth is on the order of 10^5 kg/day, hence the Moon is expected to be bombarded by 5×10^3 kg/day of IDPs arriving with a characteristic speed of 20 km/s (Taylor, 1996).

High-speed dust impacts into solid surfaces generate plasma (Dietzel et al., 1973) and neutral (Collette et al., 2014) gas clouds, as well as solid secondary ejecta dust particles (Hartmann, 1985). Ejecta particles with sufficient speeds escape from their parent body and have been identified as sources of planetary rings at Jupiter (Ockert-Bell et al., 1999), for example. Particles ejected with speeds below the escape speed follow bound orbits and return to the surface. Before LDEX visited the Moon, bound ejecta clouds forming dust exospheres were observed only around the icy moons of Jupiter (Krüger et al., 1999) and Saturn's moon Enceladus, though in the latter case active geysers are the dominant source of particles (Spahn et al., 2006). LDEX has since confirmed the existence of an asymmetric dusty exosphere engulfing the Moon, which responds to the local influx of micrometeoroids bombarding the lunar surface (Horányi et al., 2015).

Fully characterizing the meteoroid environment at 1 AU remains a challenging and active area of research. Meteoroid influx at Earth is measured via ground-based visual (Jenniskens, 1994) and radar observations (Brown et al., 2008; Campbell-Brown, 2008), which are highly sensitive to the mass and speed of incoming particles. Until LADEE, meteoroid flux to the lunar surface was monitored by visual light flash observations from large impactors with masses > 1 kg (Suggs et al., 2014). Meteoroid influx was also measured by the Apollo lunar seismic station, which operated from 1969 to 1977 and had an estimated mass sensitivity of 10^{-1} to 10^3 kg (Oberst and Nakamura, 1991) The previous lunar impact observations were able to detect much larger impacts than those that regularly sustain the lunar dust cloud given the larger cross sectional detection area required to measure an appreciable number of such impacts. The Moon acts as a large area dust detector, amplifying the amount of material impacting its surface by ejecting significantly more mass as outgoing solid ejecta (Horányi et al., 2015). LDEX measured the distribution of this impact generated

* Corresponding author at: Southwest Research Institute, 6220 Culebra Rd, San Antonio, TX 78238, USA. Tel.: +1 2105223723.
E-mail address: jszalay@swri.edu (J.R. Szalay).

http://dx.doi.org/10.1016/j.icarus.2016.04.024

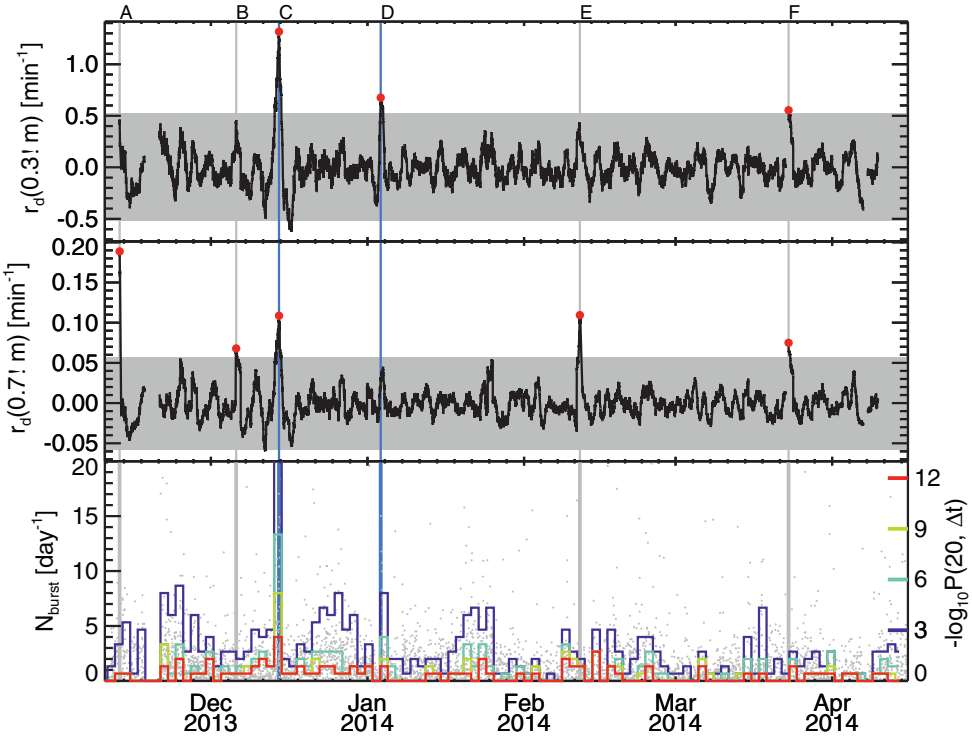

Fig. 1. LDEX impact rates and Poisson probabilities for the duration of the mission. Top and middle: The difference between 1 day and 1 week rolling averages of the impact rate as a function of time for $a > 0.3$ & 0.7 μm, respectively. The gray bar indicates 3σ error bars. Peak rates which exceed 3σ are indicated by red dots. Bottom: Gray dots show $\gamma(20, \Delta t)$ evaluated for each consecutive 20 impacts. A 1.5 day running histogram shows the total number of bursts for probability cuts of $\gamma_0 = 3$; 6; 9; and 12; in purple, indigo, yellow, and red, respectively. The 6 unusual periods which satisfy Criteria 1 (gray) or both Criteria (blue) are shown with the vertical lines, labeled A–F. (For interpretation of the references to color in this figure legend, the reader is referred to the web version of this article).

ejecta cloud and provided a novel way of observing the meteoroid influx to the Earth–Moon system.

1.1. The dust environment at the Moon

The dust environment at 1 AU is dominated by grains shed from asteroids and comets mainly within the orbit of Jupiter. These sources include comets, both long period Halley Type Comets (HTC) and short period Jupiter Family Comets (JFC), asteroids, Oort Cloud Comets (OCC), and the Edgeworth-Kuiper Belt (EKB). At 1 AU, the population of EKB grains is negligible, as most of these grains get ejected from the solar system by Jupiter during their migration towards the Sun (Han et al., 2011; Poppe, 2016). This dust/meteoroid environment is broken up into 2 distinct groups, the meteoroid streams and the sporadic background.

1.1.1. Meteoroid streams

When grains are shed, their initial orbital elements are similar to their parent body's. In addition to the gravitational forces by the Sun and the planets, the dynamics of a small dust particle is influenced by additional forces that are size-dependent, including solar wind and Poynting–Robertson drags, radiation pressure, and the Lorentz force (Han et al., 2011). The combination of these forces causes the ejected grains to decouple from their parent bodies and follow divergent trajectories over time. However, large enough (radii > 100 μm) grains preferentially disperse along the trajectory of their parent body, and may fill its entire orbital loop (Fox et al., 1983).

Once the orbit of a source body has been filled and becomes a 3D 'tube of material', it becomes a meteor stream if the orbit of the Earth intersects the ascending or descending node of this tube. There are hundreds of cataloged meteor showers, including the Geminids producing one of the strongest responses at Earth, first documented in 1862 (Fox et al., 1982; King, 1926).

1.1.2. The sporadic background

Smaller grains that are more susceptible to non-gravitational perturbations disperse, and follow orbits that rapidly diverge from their parent body, forming the 'sporadic background.' The sporadic background has its own structure and is organized by various radiant groupings: (a) the helion/anti-helion; (b) apex/anti-apex; and (c) the northern/southern toroidal sources (Jones and Brown, 1993). The relative contributions from each source vary as a function of solar longitude (Campbell-Brown and Jones, 2006). The variation of the sporadic background fluxes influences the spatial and temporal distribution of the dust ejecta cloud they generate impacting the Moon (Szalay and Horányi, 2015).

2. Impact ejecta plumes

When micrometeoroids impact the lunar surface, an ejecta plume is created that has many times the mass of the impacting particle. For normal impacts on a purely silica surface, the mass yield Y, the ratio of the mass ejected into the plume to the mass of the impacting particle is

$$Y \simeq C m_{imp}^{\alpha} v_{imp}^{\beta} \cos^2 \varphi, \quad (1)$$

where C=30 for a silicate surface, m_{imp} is the mass of the impacting particle in kg, and v_{imp} is the velocity of the impacting particle in km/s, $\alpha = 0.2$, and $\beta = 2.5$ (Koschny and Grün, 2001; Krivov et al., 2003). The angular dependence is derived from an experimental finding that the material excavated by impacts varies as $\cos^2\varphi$ where φ is angle between the surface normal and the velocity of the incoming particle (Gault, 1973). While this experiment (Gault, 1973) was performed for impacts into solid rock, which may have different impact physics compared to regolith, we still

Table 1
Enhanced Burst Activity Periods. The period corresponds to those labeled in Fig. 1. $a(\gamma_0) = N_{burst}/N_{sp}$ gives the ratio of the number of bursts in each period with the average number of sporadic bursts with the exception of the first row of data, which gives the sporadic background burst rates N_{sp}, in day^{-1}. The associated stream or complex which is temporally coincident with each period is given in the last column.

Period	LDEX Peak Time	$a(3)$	$a(6)$	$a(9)$	$a(12)$	Criteria	Associated Stream or Complex
		2.6	1.0	0.7	0.5		Sporadic Background
A	12-Nov-2013 22:10	1.3	0.6	1.0	1.3	✓	Taurid Complex
B	06-Dec-2013 00:00	0.8	1.3	1.0	1.3	✓	Puppid-Velorids I Complex
C	14-Dec-2013 11:34	10.3	13.0	12.1	7.8	✓✓	Geminids
D	03-Jan-2014 14:50	3.1	3.9	3.0	2.6	✓✓	Quandrantids
E	12-Feb-2014 01:11	0.8	1.3	2.0	2.6	✓	Centaurid I/II Complex
F	25-Mar-2014 08:54	1.0	1.9	2.0	2.6	✓	?

Table 2
Working List of Visual Meteor Showers from the International Meteor Organization (McBeath, 2015) during the LADEE operational period.

Name	ID	Start Time [UTC]	Stop Time [UTC]	Peak Time (Moon) [UTC]	α [deg]	δ [deg]	v [km/s]	ZHR [hr^{-1}]
Northern Taurids	NTa	20-Oct-2013	10-Dec-2013	12-Nov-2013 10:13	58	22	29	5
Leonids	Leo	06-Nov-2013	30-Nov-2013	17-Nov-2013 15:50	152	22	71	15
α-Monocerotids	aMo	15-Nov-2013	25-Nov-2013	21-Nov-2013 16:11	117	1	65	Var
Phoenicids	Pho	28-Nov-2013	09-Dec-2013	06-Dec-2013 09:57	18	−53	18	Var
Puppid/Velids	Pup	01-Dec-2013	15-Dec-2013	07-Dec-2013 03:41	123	−45	40	10
Monocerotids	Mon	27-Nov-2013	17-Dec-2013	09-Dec-2013 02:56	100	8	42	2
σ-Hydrids	sHy	03-Dec-2013	15-Dec-2013	12-Dec-2013 01:48	127	2	58	3
Geminids	Gem	04-Dec-2013	17-Dec-2013	14-Dec-2013 05:44	112	33	35	120
Comae Berenicids	CBe	12-Dec-2013	23-Dec-2013	19-Dec-2013 22:34	175	18	65	3
Urside	Urs	17-Dec-2013	26-Dec-2013	22-Dec-2013 14:14	217	76	33	10
Quadrantids	Qua	28-Dec-2013	12-Jan-2014	03-Jan-2014 19:39	230	49	41	120
α-Centaurids	aCe	28-Jan-2014	21-Feb-2014	08-Feb-2014 06:07	210	−59	56	6
Omicron Centaurids*	oCe	09-Feb-2014	13-Feb-2014	11-Feb-2014 17:07	175	−55	51	2
γ-Normids	gNo	25-Feb-2014	22-Mar-2014	14-Mar-2014 20:55	239	−50	56	6

*The Omicron Centaurids (oCe) is a weaker shower and was added to this list due to its temporal correlation with an observed peak. The peak times have been adjusted from the peak times observed at Earth by taking into account the position of the Moon relative to Earth and correcting for the appropriate lead/lag times.

implement its results as it is the most relevant finding on the angular dependence of impact ejecta.

The total mass production per unit area in kg/m^2 is given by $M^+ = F_{\rm imp} m_{\rm imp} \cos(\varphi) Y$ where $F_{\rm imp}$ is the number flux of impactors per square meter with characteristic mass $m_{\rm imp}$, $\cos\varphi$ is the projection area factor, and Y is from Eq. 1. Hence the total mass production per unit area is,

$$M^+ = C F_{\rm imp} v_{imp}^{\beta} m_{imp}^{\alpha+1} \cos^3\varphi. \quad (2)$$

The Moon is continually bombarded by IDPs forming meteoroid streams, as well as the sporadic background. Surface regions that are transiently exposed to higher than average IDP fluxes respond with an increased mass production M^+ during these periods, and generate more frequent and denser ejecta plumes. If LADEE happens to fly through any of these plumes it is expected to observe higher than average impact rates. Hence, a period of unusually large impact rates detected by LDEX can be used to identify the surface region that has been exposed to high incoming IDP fluxes during that period.

3. Burst detections

3.1. Identification of unusual periods

LDEX is an impact ionization dust detector. Particles are detected by measuring the charge they generate impacting the target surface (Horányi et al., 2014). The conversion from impact charge to radius is based on laboratory calibrations (Horányi et al., 2014). With an average impact speed of $\simeq$ 1.67 km/s, LADEE's orbital speed around the Moon, LDEX can detect particles as small as $a \simeq 0.3\,\mu$m in radius.

LDEX received impacts above its detection threshold of $a > 0.3\,\mu$m at a rate of $\mu = 2.3 \times 10^{-2}$ s^{-1} during commissioning and $\mu = 3.1 \times 10^{-2}$ s^{-1} during the nominal science mission, which began on 21-Nov-2013 (Horányi et al., 2015). However, intermittently, LDEX detected "bursts" of tens to hundreds of impacts in a single minute. Particles detected in a burst most likely originate from the same well-timed and well-positioned lunar impact event that occurred just minutes before their detection on the ground-track of LADEE. These bursts are detections of individual ejecta plumes, dense enough to register multiple impacts on LDEX as it transits the plume, and have durations of less than a minute. Plasma events occasionally registered false triggers on the LDEX instrument, which also manifests in bursts of detections. These events are removed from the dataset given their identifiable waveform characteristics. For more information on waveform processing, see Horányi et al. (2014).

To characterize these bursts, we assume that subsequent impacts are independent of each other, hence the dust detection time series observed by LDEX can be approximated as a Poisson process. The probability of detecting n or more impacts within a time Δt can be calculated (Oberst and Nakamura, 1991)

$$P(n, \Delta t) = 1 - e^{-\mu \Delta t} \sum_{n'=0}^{n-2} (\mu \Delta t)^{n'} / n'!, \quad (3)$$

where n is the number of impacts, Δt is the total elapsed time for the impacts, and μ is the average impact rate for the entire time series of dust detections. The upper limit of $n-2$ in the summation is due to the fact that Δt begins and ends at individual particle detections. For example the probability of detecting 2 or more particles separated by time Δt is $P(2, \Delta t) = 1 - e^{-\mu \Delta t}$, as expected.

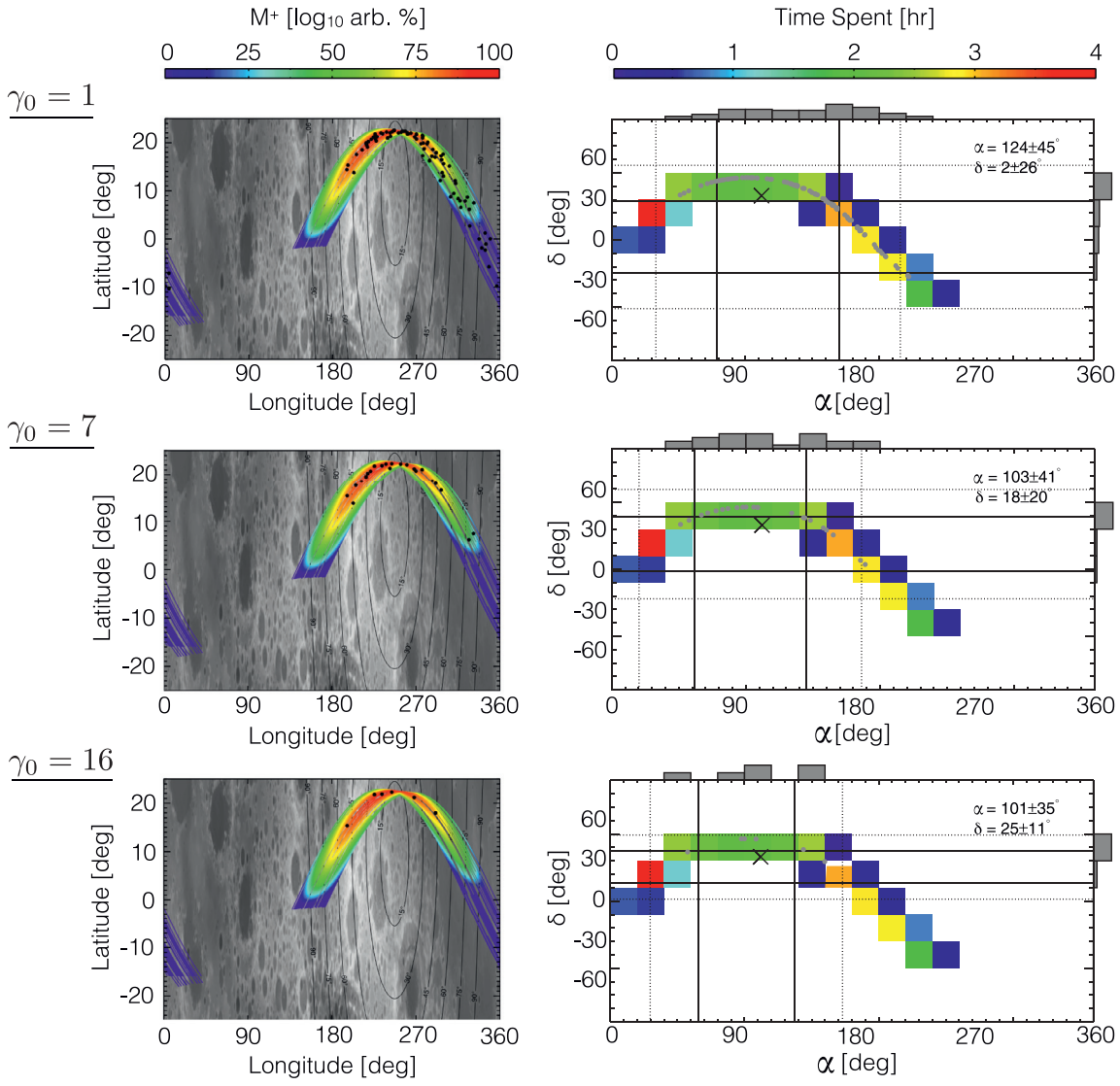

Fig. 2. The burst distributions for probability cuts $\gamma_0 = 1, 7,$ and 16, showing the correlation between γ_0 and the distribution of bursts around peak Geminids M^+. *Left column:* The LADEE trajectory for ± 1.5 days centered around the peak Geminids time, colored by M^+ from Eq. 2. Black dots mark the locations of bursts observed by LDEX, and the black contour lines show the angle φ of impact for the incident Geminids particles with respect to the surface normal. *Right column:* The α and δ distributions for the bursts (gray dots). The color bar indicates the time spent in each [α, δ] bin and the gray histograms on the top/right of each panel show the number of bursts per bin. The solid and dotted lines mark 1σ and 2σ error bars respectively, calculated using the distribution of detected bursts normalized by the LDEX observation time, and the large x marks the Earth-observed radiant (McBeath, 2015).

Bursts are short unusual periods that are identified in our time series analysis by setting an optimum value for n, a measure of the number of impacts on LDEX resulting from each burst, and identifying the low probability periods (Oberst and Nakamura, 1991). With n set to large values ($n \gg 20$), many bursts will be missed as the bursts LDEX detected contained considerably smaller numbers of particles, including additional impacts from the background raises the probability towards the average. A small value of n identifies too many unusual periods, and makes it cumbersome to recognize if they actually belong to a single impact with a larger number of particles. With values of n near 20, the results are not particularly sensitive to n. We found $n = 20$ to be a convenient particle number per burst for this analysis, using the most active period discussed below as a training set to determine this number. Unless stated otherwise, $P = P(n, \Delta t)$ with $n = 20$ will be used through the remainder of this analysis. Given the broad range in the exponent of the probabilities used in this analysis, it is convenient to express $P = 10^{-\gamma}$ in terms of its exponent $\gamma = -\log_{10} P$. Fig. 1 shows γ for each consecutive 20 impact detections. If more than 20 impacts occur in a given burst, only the first 20 are counted. Any impacts occurring less than 30 s after a burst of 20 particles are considered part of this burst and removed from the analysis.

To identify unusual periods in the LDEX data, we set 2 criteria:

(1) The impact rate deviation r_d exceeds 3σ above the average, either for $a > 0.3$ or 0.7 μm
(2) The detected burst rate N_{burst} (given in Table 1) for $a > 0.3\,\mu$m exceeds the average sporadic background N_{sp} by a factor of 3.

The impact rate deviation r_d is calculated by $r_d = r_{\text{day}} - r_{\text{week}}$ where r_{day} and r_{week} are running averages of the impact rates over a period of 1 day and 1 week, respectively. The 1 week average gives an estimate of the background to be subtracted from the impact rates, and 3σ is chosen to identify particularly unusual

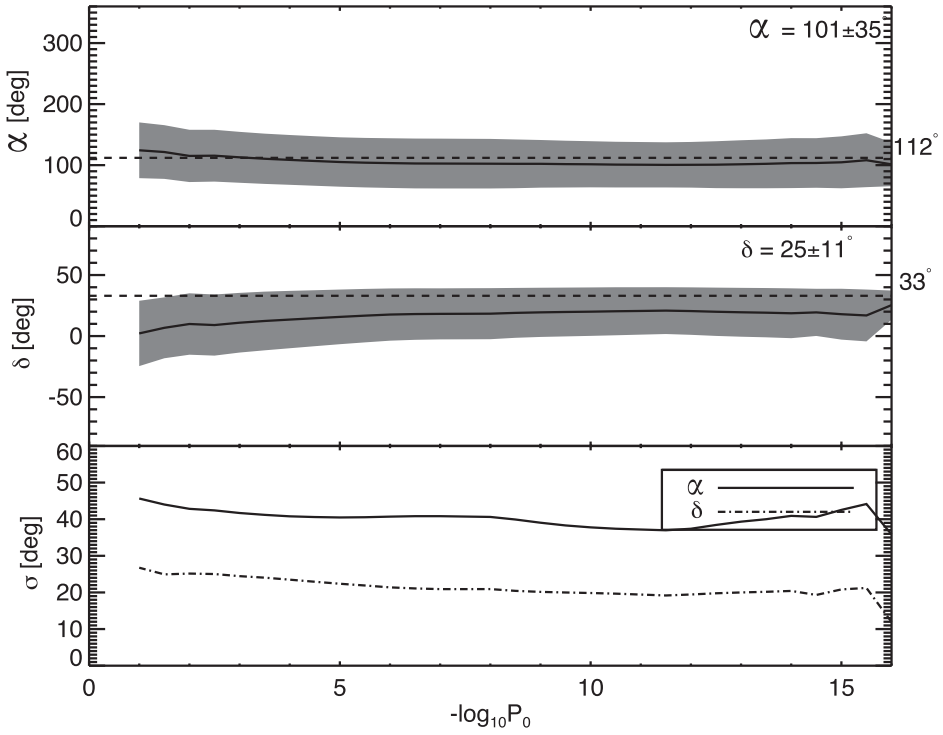

Fig. 3. The α (*top panel*) and δ (*middle*) values respectively for the bursts measured during the Geminids shower, as a function of $\gamma_0 = -\log_{10}P_0$. The solid line indicates the mean value and the gray band shows 1σ error. The horizontal dotted lines indicate the Earth observed radiant values (McBeath, 2015). *Bottom:* The 1σ error for α and δ.

periods. LDEX occasionally observed bursts with atypical size distributions, some of which had significantly more larger particles than the dust cloud. Due to this variation, two size cuts (0.3 and 0.7 μm) are utilized to ensure impact rate enhancements are detected even if bursts have different size distributions.

The sporadic rate, N_{sp}, is determined by taking the average burst rate for bursts with $\gamma > \gamma_0$ and is listed in Table 1 for $\gamma_0 = 3; 6; 9;$ and 12. Fig. 1 shows r_d for both size cutoffs of $a >$ 0.3&0.7 μm, and the burst detection rate N_{burst} for the same four γ_0 values.

3.2. Correlation with established meteoroid streams

Table 2 lists the known meteoroid showers determined by visual observations given by the International Meteor Organization (McBeath, 2015). Table 1 shows each identified unusual period along with their peak time and associated stream which coincides with each. With the exception of period F, each identified period occurs during a known meteoroid shower. However, temporal coincidence alone is not sufficient to establish the detection of a meteoroid shower. If a meteoroid stream impacts the Moon on the opposite hemisphere to where the concentration of bursts were to occur, it cannot be responsible for the burst rate enhancement. For an unusual burst activity period an estimated radiant can be calculated, and at a minimum, it must be pointing to within the same hemisphere as the temporarily coincident known shower to be classified as a potential meteoroid shower detection.

4. Radiant determination

During Period C, LDEX observed the largest burst rate enhancement, 8–13 times greater than the sporadic background. We therefore first focus on this period to establish a method to find the radiant of the responsible meteoroid shower. A right ascension, α, and declination, δ, are calculated for each burst by determining the radiant which intersects the burst location normal to the lunar surface. We use the period of ± 1.5 days centered around each peak time, as this was approximately the duration of each period of elevated impacted rates (Table 1).

LDEX's observed impact rates peaked during Period C on 14-Dec-2013 11:34 [UTC]. The expected peak flux from the Geminids was 14-Dec-2013 7:49, less than 4 h (or 2 LADEE orbits) apart. The Geminids is a well constrained and intense shower, its radiant is established precisely by ground-based visual observations.

Fig. 2 shows the distribution of bursts detected by LDEX during Period C for an increasing set of γ_0 values. To a good approximation, the meteoroids arrive at the Moon in a parallel beam, hence the theoretical M^+ given in Eq. 2 can be calculated. We show M^+ in normalized units, such that it is strictly proportional to $\cos^3\varphi$. For $\gamma_0 = 1$ the burst distribution remains isotropic. This is to be expected as 10% probability events are likely to be related to background sporadic impacts. For $\gamma_0 = 7$, the remaining bursts tend to concentrate around higher M^+ regions, and for $\gamma_0 = 16$, only the most unusual bursts remain, identifying the most dense ejecta plumes.

Fig. 2 demonstrates that increasing γ_0 (decreasing the probability cut) gives increasingly better estimates for the radiant, hence it can be used to extract the direction information for a meteoroid stream. Using γ as a proxy for the density of each measured plume, such that higher values of γ indicate lower probability events and therefore higher plume densities, we analyzed the RA and δ distributions as a function of γ_0. Bursts with larger γ are generated in regions of higher M^+ and therefore as γ_0 increases, the corresponding radiant estimates becomes more accurate. Fig. 3 shows the mean and standard deviations for $\alpha(\gamma_0)$ and $\delta(\gamma_0)$. We use the largest γ_0 with at least 3 remaining bursts to determine the best value for RA and δ, $\gamma_0 = 16$ in the case of the Geminids. For $\gamma_0 > 16$, we observed no considerable change in burst distributions. With $\gamma_0 = 16$, we estimate the Geminids radiant within 1σ as $(\alpha, \delta) = (92 \pm 31°, 27 \pm 8°)$ compared to the

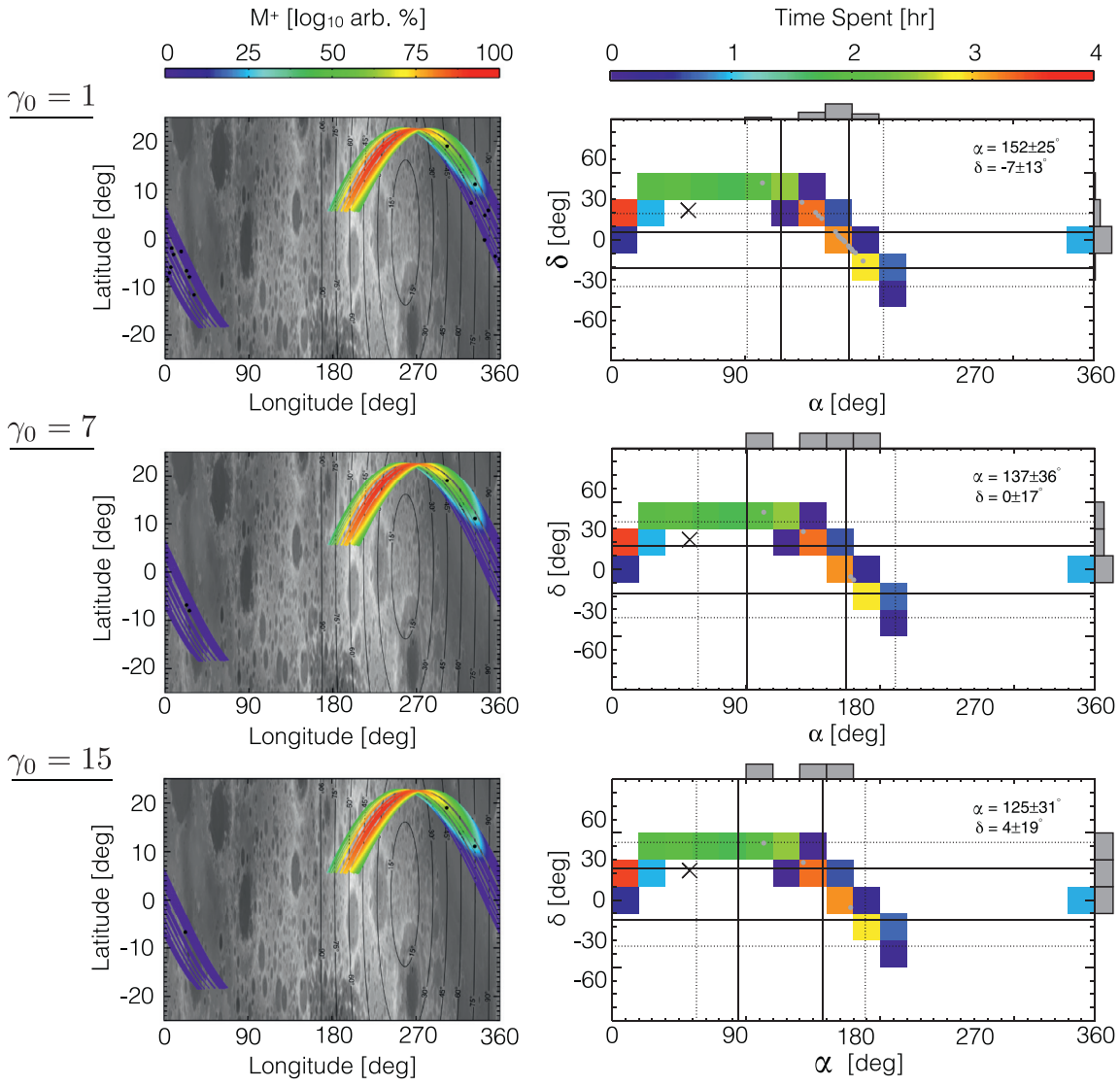

Fig. 4. The burst distributions during Period A for $\gamma_0 = [1, 7, 15]$, corresponding to the Northern Taurids. See Fig. 2 caption for further explanation.

established radiant of (112°, 33°) (McBeath, 2015). Therefore, the burst rate enhancement during Period C was indeed due to the Geminids meteoroid stream.

5. Application to additional periods

The analysis outlined in the previous section provides a method to calculate the radiant of a meteoroid shower for sufficiently large number of burst detections. However, even the most intense showers can escape detection by this method if their radiant intersects the lunar surface far outside LADEE's selenographic latitude range of ± 23°. The Geminids hit the lunar surface in an optimal location for LADEE's orbital geometry and generated bursts at a rate up to 13 times higher than the sporadic background. This shower, corresponding to Period C, stands out in the LDEX data as the strongest stream detection. The remaining unusual periods are discussed below and compared to temporally coincident known meteoroid streams.

5.1. Period A: Northern Taurids

During this period, LDEX recorded one of the largest impact rate enhancements, second only to the Geminids during Period C. However, unlike the Geminids, which generated a burst rate enhancement of $a = N_{burst}/N_{sp} \leq 13$, an enhancement of $a \leq 1.3$ was registered during Period A (Table 1). The bursts measured during this period were unusually dense, with γ values up to 15. Fig. 4 shows the burst distributions during this period. The declination is correctly estimated, however the right ascension is not. The Northern Taurids have a ZHR which is 24 times less than the Geminids and are therefore expected to impact the Moon at a much lower rate.

5.2. Period B: Puppid/Velids

The Puppid/Velids stream is also known to be weak, with a ZHR of 10, and at most registered a burst rate 1.3 times the sporadic burst rate. Additionally, its radiant impacts the lunar surface at a low selenographic longitude of −45°. Due to the geometry of the LADEE orbit, throughout each orbit LDEX essentially flys through iso-M^+ or iso-φ lines, as shown in Fig. 5. Given this geometry and the relative weakness of the stream, extracting the radiant for this stream is difficult, but still its declination is correctly estimated.

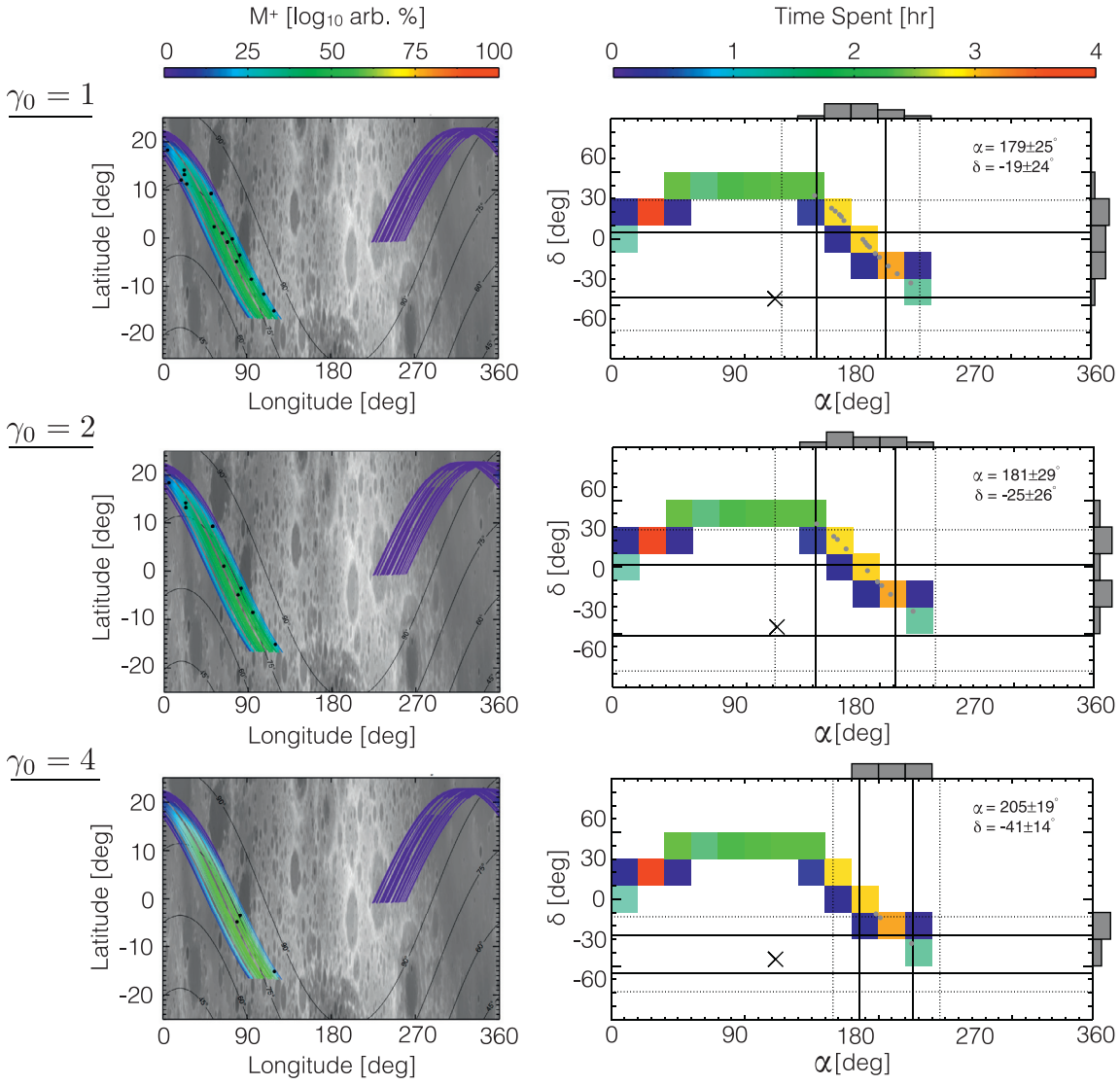

Fig. 5. The burst distributions during Period B for $\gamma_0 = [1, 2, 4]$, corresponding to the Puppid/Velids. See Fig. 2 caption for further explanation.

5.3. Period D: Quadrantids

The Quadrantids is one of the strongest observed showers on Earth, similar in ZHR magnitude to the Geminids, and was predicted to peak approximately 6.5 h after LDEX's observed peak in Period D. Fig. 6 shows the burst distributions during this period. The radiant of this stream intersected the lunar surface at a very high lunar latitude, 63° in selenographic coordinates. Due to the geometry, the declination for this radiant cannot be accurately determined as LDEX did not visit the relevant δ range. However, LDEX did visit a large range of α in this period and an accurate estimate for the α can be extracted from the data.

5.4. Period E: Omicron Centaurids

An additional stream which generated a significant enhancement in LDEX impact rates, as shown in Fig. 1, was the Omicron Centaurids (oCe). Like the Quadrantids, this stream intersected the lunar surface at an unfavorable selenographic latitude of −51° (Fig. 7). Due to the unfavorable geometry and lower burst rate enhancement for this period of 0.8 to 2.6, radiant estimation was challenging.

5.5. Period F: Unidentified

Several of the documented streams produced significant enhancements in impact rate at the expected time. Surprisingly, an uncharacteristically large impact rate enhancement, rivaling the Geminids, was also observed on 25-Mar-2014 that does not correspond to any established shower. If this impact rate enhancement is due to a meteoroid shower, its radiant can be estimated following the analysis outlined in the previous sections.

Fig. 8 shows the burst distribution for this period. For the largest cut of $\gamma_0 = 5$, a radiant estimate is calculated as (α, δ) = (268 ± 41°, −22 ± 13°) and the local impact rate maximum gives $\lambda = 4.1 \pm 0.3°$. The constellation in the sky at this radiant is Sagittarius, hence this stream could be named the Sagittarids (Sag). Fig. 8 shows the burst distribution for this unidentified stream.

Of all documented meteoroid streams, the only candidate stream with possibly similar temporal and spatial parameters to the unidentified stream on 25-Mar-2014 is the ζ-Serpentids

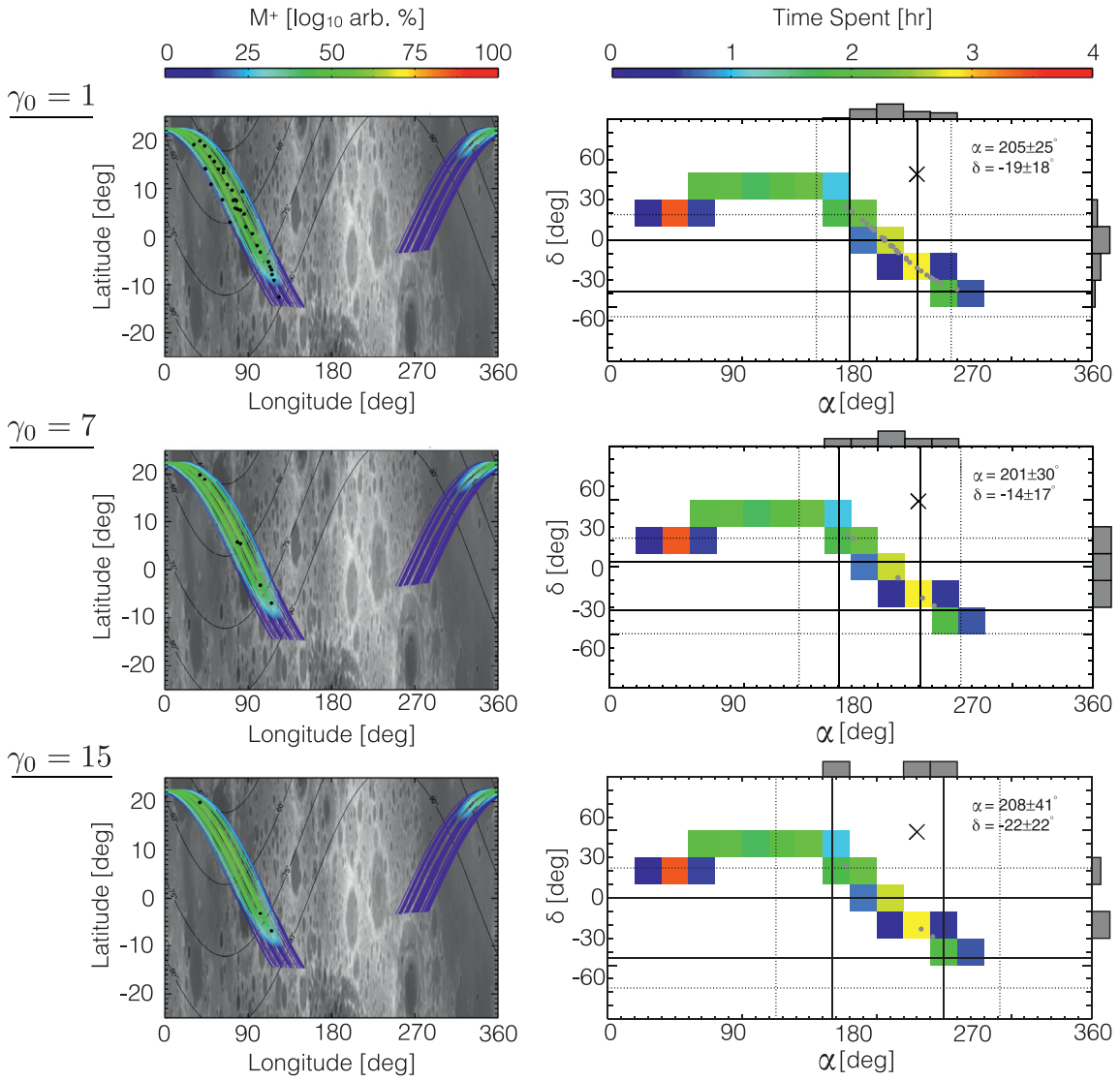

Fig. 6. The burst distributions during Period D, corresponding to the Quadrantids for γ_0 = [1, 7, 15]. See Fig. 2 caption for further explanation.

shower. However, this stream is relatively weak and remains fairly unconstrained. The Meteor Data Center (Porubcan and Jopek, 2015) gives the following radiant parameters: λ=5° and (α, δ) = (266°, −6.3°). The α value is within 1σ of the LDEX calculated radiant, with δ within 2σ and λ is within 1° (or one day) of the observed lunar peak time. However, the SonotaCo meteor orbit database gives a solar longitude for the ζ-Serpentids of λ=365°, with (α, δ) = (266°, −6°) (Greaves, 2012). The radiant direction given in Greaves (2012) could be consistent with the LDEX results, however the solar longitude is considerably different. Additionally, the lunar response to the unidentified stream is similar to the intense impact rates observed during the Geminids. This is not consistent with the low magnitude of the ζ-Serpentids which remains poorly characterized by ground-based observations.

6. Discussion

Table 3 summarizes the LDEX radiant estimates of the meteoroid showers. Of the 6 identified periods, the Geminids produced the largest burst rate enhancement. The LDEX data from this period unambiguously verifies the detection of the lunar response and successfully extracts both radiant parameters as well as the peak time. LDEX can only resolve a maximum in impact rate within a few LADEE orbits. Here, we use 3 orbits as our error criteria, corresponding to approximately 6 h or 0.3° in solar longitude. For Periods A, B, D, and E, which correlate temporally to known showers, the radiant estimates were more difficult to extract. These difficulties arose from unfavorable geometry, low relative meteoroid stream strength, or both. The Quadrantids, which is comparable in magnitude to the Geminids as observed at Earth, generated the 2nd highest burst rate detected throughout the mission. However, due to its high selenographic latitude, it's declination can only be poorly reproduced.

Many of the streams listed in Table 2 did not generate significant burst rate enhancements. While the non-detection of these streams is largely unsurprising due to their low ZHR, the Leonids is strongest amongst these and should have registered a burst rate enhancement given the favorable geometry and its larger ZHR. However, LDEX turned off a few hours before the Leonids peak time and remained off for a few days due to spacecraft operational constraints, therefore missing this stream.

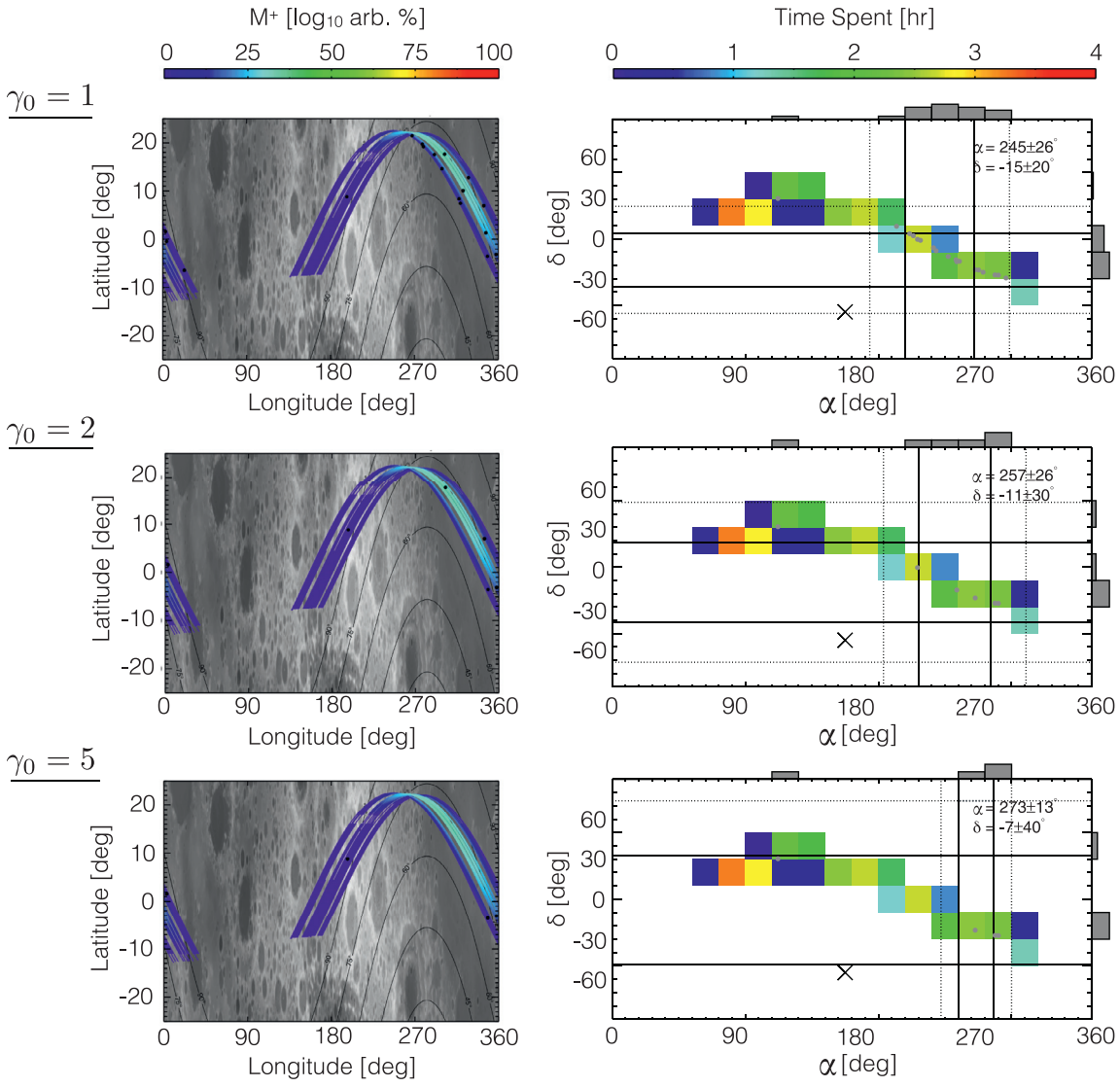

Fig. 7. The burst distributions during Period E, corresponding to the Omicron Centaurids for $\gamma_0 = [1, 2, 5]$. See Fig. 2 caption for further explanation.

Table 3
Extracted Meteoroid Stream Parameters. The established three letter identification code is id, λ is the peak time in solar longitude, RA is right ascension, δ is the declination, and $N(3)$ is the number of bursts with a probability cut of $\gamma_0 = 3$. Earth observed values (McBeath, 2015), propagated in time to the position of the Moon at each peak time. The error on λ for LDEX measured values was calculated assuming LDEX could not resolve a maximum in impact rate within three LADEE orbits, corresponding to approximately 6 h or 0.3° in solar longitude. Highlighted in bold are the values for which the estimates are within 1σ.

Per.	id	Lat [deg]	λ [deg]	λ_{LDEX} [deg]	α [deg]	α_{LDEX} [deg]	δ [deg]	δ_{LDEX} [deg]	$N(3)$ [day^{-1}]
A	NTa	1	227.7	**227.8 ± .3**	58	118 ± 38	22	−5 ± 27	3.3
B	PuV	−64	253.8	252.5 ± .3	123	205 ± 19	−45	**−41 ± 14**	2.0
C	Gem	10	261.6	**261.8 ± .3**	112	**92 ± 31**	33	**27 ± 8**	26.7
D	Qua	63	284.4	**284.6 ± .3**	230	**225 ± 12**	49	−25 ± 17	8.0
E	oCe	−50	325.1	**325.4 ± .3**	175	273 ± 13	−55	−7 ± 40	2.0
F				4.1 ± .3		275 ± 38		−23 ± 13	2.7

In addition to the six periods discussed in this work, we note there are two additional periods which fell just shy of our identification criteria, Nov. 24–28, 2013 and Jan. 22–27, 2014. As discussed in depth in Szalay and Horányi (2015), the majority of the ejecta detected by LDEX was from three sporadic meteoroid sources, helion, apex, and anti-helion. The apex source was found to be the most dominant producer of impact ejecta due to its large impact velocity. The two additional periods not marked on Fig. 1 are enhancements in approximately the apex direction. These enhancements could be from random fluctuations in the apex source, or additional unidentified meteoroid streams, weaker than that of Period F.

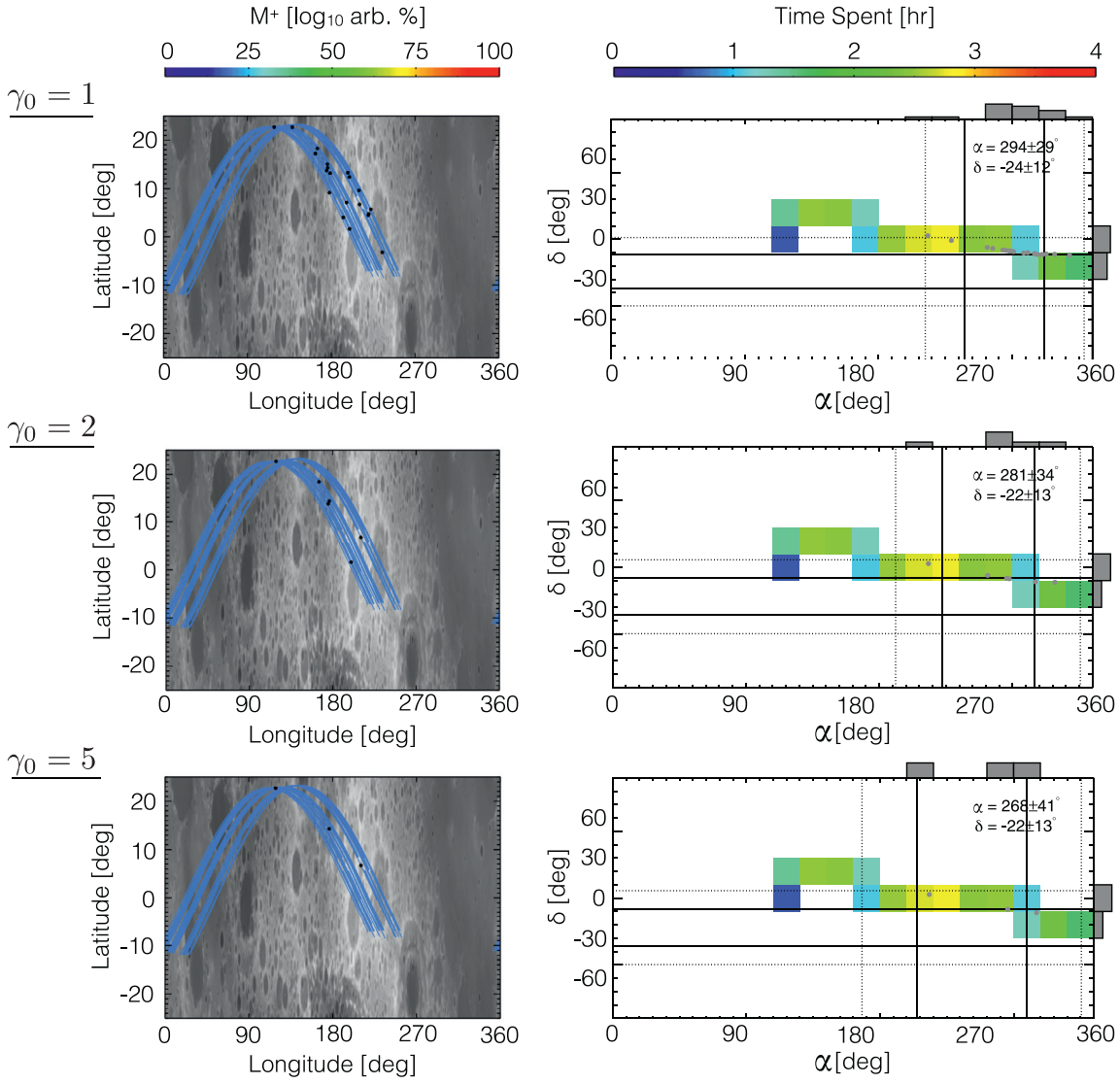

Fig. 8. The burst distributions during Period F for $\gamma_0 = [1, 2, 5]$. For $\gamma_0 > 5$, there were less than 3 bursts. See Fig. 2 caption for further explanation.

7. Conclusions

Using Poisson statistical methods to quantitatively identify unusual periods in the LDEX impact rate data, a method similar to that outlined in Oberst and Nakamura (1991) is proposed to characterize meteoroid streams. By analyzing the distribution of right ascension and declination of groupings of impacts, the radiant for a strong and established meteoroid stream (the Geminids) was successfully reproduced within 1σ error. Partial radiants and/or peak times are correctly estimated for 4 other meteoroid streams.

An unidentified meteoroid stream is observed by the LDEX instrument aboard the LADEE mission, peaking on 25-Mar-2014. Using the methods outlined in this work, an estimate for the radiant of this putative stream is calculated as $(\alpha, \delta) = (268 \pm 41°, -22 \pm 13°)$, with a peak solar longitude of $\lambda = 4.1 \pm 0.3°$. However, this radiant estimate may not be reliable due to geometric constraints. Additionally, while LDEX observed a handful of dense ejecta plumes during this period, the rate of detected bursts was not significantly higher than the sporadic background.

Detecting and measuring the orbital properties of meteoroid streams is currently undertaken via multiple methods, each with its own strengths and weaknesses. The meteoroid stream characterization outlined in this work provides a novel method to measure the local meteoroid environment using the Moon as large surface area dust detector, by exploiting the large magnification factor in the density of the ejecta plumes. Future longer duration lunar missions carrying an LDEX type instrument, and following orbits with higher inclinations than LADEE could greatly enhance our knowledge about the meteoroid environment at 1 AU. Spacecraft carrying a dust instrument orbiting, or performing multiple flybys, of other airless bodies could be used to learn about the meteoroid environment throughout the solar system in a manner unique to dust detectors.

Acknowledgments

All LDEX data are available through NASA's Planetary Data System (http://sbn.psi.edu/pds/resource/ldex.html). J. Szalay was supported by NASA's Earth and Space Science Graduate Fellowship Program (NNX12AN85H). M. Horányi was supported by NASA's LADEE mission, and the Institute for Modeling Plasma, Atmospheres, and Cosmic Dust (IMPACT) of NASA's Solar System Exploration Research Virtual Institute (SSERVI). The authors thank Eberhard Grün and Rachel Soja for insightful discussions on the meteoroid environment at 1 AU.

References

Brown, P., Weryk, R., Wong, D.K., et al., 2008. A meteoroid stream survey using the Canadian meteor orbit radar. I. Methodology and radiant catalogue. Icarus 195 (1), 317–339.

Campbell-Brown, M., Jones, J., 2006. Annual variation of sporadic radar meteor rates. Mon. Not. R. Astron. Soc. 367 (2), 709–716.

Campbell-Brown, M.D., 2008. High resolution radiant distribution and orbits of sporadic radar meteoroids. Icarus 196, 144–163. doi:10.1016/j.icarus.2008.02.022.

Collette, A., Sternovsky, Z., Horányi, M., 2014. Production of neutral gas by micrometeoroid impacts. Icarus 227, 89–93. doi:10.1016/j.icarus.2013.09.009.

Dietzel, H., Eichhorn, G., Fechtig, H., et al., 1973. The HEOS 2 and HELIOS micrometeoroid experiments. J. Physics. E Sci. Instrum. 6, 209–217.

Fox, K., Williams, I.P., Hughes, D.W., 1982. The evolution of the orbit of the geminid meteor stream. Mon. Not. R. Astron. Soc. 200, 313–324.

Fox, K., Williams, I.P., Hughes, D.W., 1983. The rate profile of the geminid meteor shower. Mon. Not. R. Astron. Soc. (ISSN 0035–8711) 205, 1155–1169.

Gault, D.E., 1973. Displaced mass, depth, diameter, and effects of oblique trajectories for impact craters formed in dense crystalline rocks. Moon 6, 32–44. doi:10.1007/BF02630651.

Greaves, J., 2012. Four IAU MDC working list meteor showers confirmed via sonotaco network japan data. WGN, J. Int. Meteor Organ. 40, 53–58.

Grün, E., Zook, H.A., Fechtig, H., et al., 1985. Collisional balance of the meteoritic complex. Icarus 62, 244–272. doi:10.1016/0019-1035(85)90121-6.

Han, D., Poppe, A.R., Piquette, M., et al., 2011. Constraints on dust production in the Edgeworth-Kuiper belt from pioneer 10 and new horizons measurements. Geophys. Res. Lett. 38. doi:10.1029/2011GL050136. L24102.

Hartmann, W.K., 1985. Impact experiments. i - ejecta velocity distributions and related results from regolith targets. Icarus 63, 69–98. doi:10.1016/0019-1035(85)90021-1.

Horányi, M., Sternovsky, Z., Lankton, M., et al., 2014. The lunar dust experiment (LDEX) onboard the lunar atmosphere and dust environment explorer (LADEE) mission. Space Sci. Rev. 185, 93–113.

Horányi, M., Szalay, J.R., Kempf, S., et al., 2015. A permanent, asymmetric dust cloud around the moon. Nature 522 (7556).

Jenniskens, P., 1994. Meteor stream activity i. The annual streams. Astron. Astrophys. 287, 990–1013.

Jones, J., Brown, P., 1993. Sporadic meteor radiant distributions - orbital survey results. Mon. Not. R. Astron. Soc. 265, 524–532.

King, A., 1926. An ephemeris of the geminid radiant-point. Mon. Not. R. Astron. Soc. 86, 638–641.

Koschny, D., Grün, E., 2001. Impacts into ice-silicate mixtures: Ejecta mass and size distributions. Icarus 154, 402–411. doi:10.1006/icar.2001.6708.

Krivov, A.V., Sremčević, M., Spahn, F., et al., 2003. Impact-generated dust clouds around planetary satellites: spherically symmetric case. Planet. Space Sci. 51, 251–269.

Krüger, H., Krivov, A., Hamilton, D., et al., 1999. Detection of an impact-generated dust cloud around ganymede. Nature 399, 558–560.

McBeath, A., 2015. International meteor organization. http://www.imo.net, Accessed: 2015-09-18.

Oberst, J., Nakamura, Y., 1991. A search for clustering among the meteoroid impacts detected by the apollo lunar seismic network. Icarus 91, 315–325. doi:10.1016/0019-1035(91)90027-Q.

Ockert-Bell, M.E., Burns, J.A., Daubar, I.J., et al., 1999. The structure of jupiter's ring system as revealed by the galileo imaging experiment. Icarus 138, 188–213. doi:10.1006/icar.1998.6072.

Poppe, A.R., 2016. An improved model for interplanetary dust fluxes in the outer Solar System. Icarus 264 (C), 369–386. doi:10.1016/j.icarus.2015.10.001.

Porubcan, V. Jopek, T., 2015. Meteor data center. http://www.astro.amu.edu.pl/~jopek/MDC2007/index.php, accessed: 2015-04-23.

Spahn, F., Schmidt, J., Albers, N., et al., 2006. Cassini dust measurements at enceladus and implications for the origin of the e ring. Science 311, 1416–1418. doi:10.1126/science.1121375.

Suggs, R.M., Moser, D.E., Cooke, W.J., et al., 2014. The flux of kilogram-sized meteoroids from lunar impact monitoring. Icarus 238, 23–36. doi:10.1016/j.icarus.2014.04.032.

Szalay, J.R., Horányi, M., 2015. Annual variation and synodic modulation of the sporadic meteoroid flux to the moon. Geophys. Res. Lett. 42 (24), 10,580–10,584. doi:10.1002/2015GL066908. 2015GL066908.

Taylor, A.D., 1996. Earth encounter velocities for interplanetary meteoroids. Adv. Space Res. 17, 205–209. doi:10.1016/0273-1177(95)00782-A.